2011

Coupled Photonic Crystal Micro-Cavities With Ultra-Low Threshold Power For Stiumulated Raman Scattering

Qiang Liu
Old Dominion University

Zhengbiao Ouyang

Sacharia Albin
Old Dominion University

Coupled photonic crystal micro-cavities with ultra-low threshold power for stimulated Raman scattering

Qiang Liu,[1] Zhengbiao Ouyang,[2] and Sacharia Albin[1,*]

[1]Photonics Laboratory, Department of Electrical & Computer Engineering, Old Dominion University, Norfolk, Virginia 23529 USA
[2]THz Technical Research Center of Shenzhen University, Shenzhen 518060 China
[*]salbin@odu.edu

Abstract: We propose coupled cavities to realize a strong enhancement of the Raman scattering. Five sub cavities are embedded in the photonic crystals. Simulations through finite-difference time-domain (FDTD) method demonstrate that one cavity, which is used to propagate the pump beam at the optical-communication wavelength, has a Q factor as high as 1.254×10^8 and modal volume as small as $0.03\mu m^3$ $(0.3192(\lambda/n)^3)$. These parameters result in ultra-small threshold lasing power ~17.7nW and 2.58nW for Stokes and anti-Stokes respectively. The cavities are designed to support the required Stokes and anti-Stokes modal spacing in silicon. The proposed structure has the potential for sensor devices, especially for biological and medical diagnoses.

©2011 Optical Society of America

References and links

1. V. R. Almeida, C. A. Barrios, R. R. Panepucci, and M. Lipson, "All-optical control of light on a silicon chip," Nature **431**(7012), 1081–1084 (2004).
2. J. D. Joannopoulos, P. R. Villeneuve, and S. Fan, "Photonics crystals: putting a new twist on light," Nature **386**(6621), 143–149 (1997).
3. S. M. Spillane, T. J. Kippenberg, and K. J. Vahala, "Ultralow-threshold Raman laser using a spherical dielectric microcavity," Nature **415**(6872), 621–623 (2002).
4. T. J. Kippenberg's PhD thesis, "Nonlinear Optics in Ultra-high-Q Whispering Gallery Mode Micro-cavities" (California Institute of Technology, May 2004), http://www.mpq.mpg.de/k-lab/publications/TJKippenbergThesis.pdf.
5. X. Yang, and C. W. Wong, "Design of photonic band gap nanocavities for stimulated Raman amplification and lasing in monolithic silicon," Opt. Express **13**(12), 4723–4730 (2005), http://www.opticsinfobase.org/oe/abstract.cfm?URI=oe-13-12-4723.
6. Q. Quan, P. B. Deotare, and M. Lončar, "Photonic Crystal Nanobeam Cavity Strongly Coupled to the Feeding Waveguide," Appl. Phys. Lett. **96**(20), 203102 (2010).
7. Y. Akahane, T. Asano, B. S. Song, and S. Noda, "High-Q photonic nanocavity in a two-dimensional photonic crystal," Nature **425**(6961), 944–947 (2003).
8. M. Krause, H. Renner, and E. Brinkmeyer, "Analysis of Raman lasing characteristics in silicon-on-insulator waveguides," Opt. Express **12**(23), 5703–5710 (2004), http://www.opticsinfobase.org/oe/abstract.cfm?URI=oe-12-23-5703.
9. V. E. Perlin, and H. G. Winful, "Stimulated Raman Scattering in nonlinear periodic structures," Phys. Rev. A **64**(4), 043804 (2001).
10. X. D. Yang, and C. W. Wong, "Coupled-mode theory for stimulated Raman scattering in high-Q/V(m) silicon photonic band gap defect cavity lasers," Opt. Express **15**(8), 4763–4780 (2007), http://www.opticsinfobase.org/abstract.cfm?URI=oe-15-8-4763.
11. C. E. B. A. H. Stein's PhD thesis, "Stimulated Raman Scattering in Silicon Coupled Photonic Crystal Microcavity Arrays" (Universität Karlsruhe, May 2006), http://www.stanford.edu/group/nqp/jv_files/thesis/Benedikt-Thesis-RamanLaserPC-Design.pdf.
12. http://www.rsoftdesign.com/.
13. N. C. Panoiu, M. Bahl, and R. M. Osgood, Jr., "All-optical tunability of a nonlinear photonic crystal channel drop filter," Opt. Express **12**(8), 1605–1610 (2004), http://www.opticsinfobase.org/oe/abstract.cfm?URI=oe-12-8-1605.

14. C. G. Bostan, R. M. de Ridder, V. J. Gadgil, L. Kuipers, and A. Driessen, "Line-Defect Waveguides in Hexagon-Hole type Photonic Crystal Slabs: Design and Fabrication using Focused Ion Beam Technology," in *Proceedings of Symposium IEEE/LEOS Benelux Chapter* (Enschede 2003) pp. 253–256.
15. T. Xu, S. Yang, S. V. Nair, and H. E. Ruda, "Nanowire-array based photonics crystal cavity by finite-difference time domain calculations," Phys. Rev. B **75**(12), 125104 (2007).
16. S. Assefa, P. T. Rakich, P. Bienstman, S. G. Johnson, G. S. Petrich, J. D. Joannopoulos, L. A. Kolodziejski, E. P. Ippen, and H. I. Smith, "Guiding 1.5 μm light in photonic crystals based on dielectric rods," Appl. Phys. Lett. **85**(25), 6110–6112 (2004).
17. M. Tokushima, H. Yamada, and Y. Arakawa, "1.5 μm-wavelength light guiding in waveguides in square-lattice-of-rod photonic crystal slab," Appl. Phys. Lett. **84**(21), 4298–4300 (2004).
18. E. Schonbrun, M. Tinker, W. Park, and J. B. Lee, "Negative refraction in a Si-polymer photonic crystal membrane," IEEE Photon. Technol. Lett. **17**(6), 1196–1198 (2005).
19. W. Y. Chiu, T. W. Huang, Y. H. Wu, Y. J. Chan, C. H. Hou, H. T. Chien, and C. C. Chen, "A photonic crystal ring resonator formed by SOI nano-rods," Opt. Express **15**(23), 15500–15506 (2007), http://www.opticsinfobase.org/oe/abstract.cfm?URI=oe-15-23-15500.
20. R. B. Wehrspohn, H. S. kitzerow, and K. Busch, *Nanophotonic Materials: Photonic Crystals, Plasmonics, and Metamaterials* (Wiley-VCH, 2008).
21. Z. Ouyang, X. Luo, J. C. Wang, C. P. Liu, and C. J. Wu, "A combined cavity for high sensitivity THz signal detection," Proc. SPIE **6840**, 684008, 684008-8 (2007).
22. Y. Wu, X. Yang, and P. T. Leung, "Theory of microcavity-enhanced Raman gain," Opt. Lett. **24**(5), 345–347 (1999).
23. B. Min, T. J. Kippenberg, and K. J. Vahala, "Compact, fiber-compatible, cascaded Raman laser," Opt. Lett. **28**(17), 1507–1509 (2003).
24. H. B. Lin, and A. J. Campillo, "cw nonlinear optics in droplet microcavities diplaying enhanced gain," Phys. Rev. Lett. **73**(18), 2440–2443 (1994).
25. H. B. Lin, and A. J. Campillo, "Microcavity enhanced Raman gain," Opt. Commun. **133**(1–6), 287–292 (1997).
26. A. B. Matsko, A. A. Savchenkov, R. J. Letargat, V. S. Ilchenko, and L. Maleki, "On cavity modification of stimulated Raman scattering," J. Opt. B Quantum Semiclassical Opt. **5**(3), 272–278 (2003).
27. R. Claps, V. Raghunathan, D. Dimitropoulos, and B. Jalali, "Anti-Stokes Raman conversion in silicon waveguides," Opt. Express **11**(22), 2862–2872 (2003), http://www.opticsinfobase.org/oe/abstract.cfm?URI=oe-11-22-2862.
28. V. M. N. Passaro, F. Dell'Olio, B. Casamassima, and F. De Leonardis, "Guided-Wave Optical Biosensors," Sensors (Basel Switzerland) **7**(4), 508–536 (2007).
29. A. Downes, and A. Elfick, "Raman Spectroscopy and Related Techniques in Biomedicine," Sensors (Basel Switzerland) **10**(3), 1871–1889 (2010).
30. C. L. Evans, and X. S. Xie, "Coherent anti-stokes Raman scattering microscopy: chemical imaging for biology and medicine," Annu Rev Anal Chem (Palo Alto Calif) **1**(1), 883–909 (2008).

1. Introduction

Silicon is considered as one of the materials suitable for nano-photonic devices due to on-chip integration and low cost production. Passive silicon devices such as submicron silicon-on-insulator (SOI) waveguides, bends, splitters, and filters have been developed as well as integrated silicon optical modulators which use two-photon absorption (TPA) or the thermo-optic effect [1].

A photonic crystal (PC), in analogy to a semiconductor crystal, is a promising platform to build future photonic integrated devices with dimensions on the order of the operating wavelength [2]. PC has unique capability to modify photon interaction with host materials. By introducing crystal defects, one can create photonic defect states inside the bandgap that allows the design of lossless resonators. These so called PC micro-cavities, that are similar to microtoroid or microsphere silica cavities [3,4], can also be used for the implementation of stimulated Raman scattering (SRS) as proposed in Ref [5]. The lasing threshold of a Raman laser is proportional to the inverse of the quality factors of the pump and the lasing modes. This implies that PC micro-cavity resonators with high quality factors offer strong enhancement for the optical fields with wavelength at and near the localized defect mode, resulting in the potential for the design of ultra low threshold Raman lasers.

Recently, the design of photonic band gap nanocavities for stimulated Raman amplification in monolithic silicon has been proposed; however, quality factors for both the Stokes and the pump are not so high (maximum at 42445 and 1550 respectively), due to the edge effect for pump mode [5]. On the other hand, ultra-high Q silica microspheres and microtoroids that produce Raman laser have significantly reduced the threshold power of pump for SRS; however, the modal volume is still too large (200-2000 μm^3) which limits the

application toward integration. Now, experimental realization of high quality micro-cavities [6,7] has been reported, however, the question of how to use ultra-high quality micro-cavities to produce and collect Raman signals (Stokes and anti-Stokes) is still unanswered.

This paper analyzes rod-type PC Raman laser on a chip, with ultra-low threshold power of pump for both the Stokes and anti-Stokes lasing. We introduce a new structure for the implementation of SRS on silicon, the so called coupled PC micro-cavities. The structure consists of five micro-cavities based on two dimensional rod-type PC made of monolithic silicon. The coupled resonators have high quality factors and allow lasing at significantly decreased thresholds compared to that in Refs. [3–5].

In Sec. 2 of the paper, we give the theoretical basis for designing the coupled cavities for Raman lasing. Basic structures, simulation method and main operating parameters are introduced in Sec. 3. We present two designs in Sec. 4 for the system that only emits Stokes radiation while in Sec. 5, two more designs are shown for both Stokes and anti-Stokes radiations.

2. Design concept

The origin of SRS is inelastic scattering of light by optical phonons. Krause *et al.* [8] and Perlin *et al.* [9] provide a good description of the dynamics in SRS through a set of time-dependent coupled nonlinear equations. The coupled mode theory for SRS in defect cavity lasers provides the conditions necessary for efficient Raman conversion [10] that take into account most of the material parameters and cavity losses.

Our aim is Raman lasing; we wish to achieve the highest possible output and lowest possible threshold power of pump. High quality factor Q and small modal volume V_m, in optical micro-cavities offer the possibility to decrease the lasing threshold in the cavity by several orders of magnitude, as can be seen from the following equation [5]:

$$P_{th} = \frac{\pi^2 n_S n_p}{\xi g_S \lambda_S \lambda_p} \cdot \frac{V_m}{Q_S Q_p} \tag{1}$$

where P_{th} is the threshold power of the resonant pump to trigger lasing, ξ is the modal overlap, $Q_{S,p}$ the cavity quality factors, $n_{S,p}$ the refractive indices of silicon at the Stokes and pump wavelength λ_S and λ_p respectively. The Raman gain coefficients $g_{p,S}$ at the pump and Stokes frequencies are related as $g_p = g_S \cdot \lambda_S / \lambda_p$, with a range of ~20 - 76cm/GW for silicon at the C-band [8]. Note that Eq. (1) neglects all other possible absorption processes, especially for free carrier absorption due to preliminary TPA, this assumption could possibly be too optimistic. The same process can also be applicable for anti-Stokes cavity-enhancement [5], where anti-Stokes generation typically has appreciably lower scattering intensity leading to $\frac{I_{aS}}{I_S} \approx 8\%$ [11].

In our simulation, we have used Rsoft's component design suite: *Fullwave* [12]. The electric field for excitation of pump or Stokes could be defined as:

$$\mathbf{E}_{p,S}(\mathbf{r},t) = \sqrt{P_{p,S}} \cdot G_{p,S}(\mathbf{r}) \cdot T_{p,S}(t) \tag{2}$$

where $P_{p,S}$, $G_{p,S}$, $T_{p,S}$ are respectively the power (electro-magnetic energy), spatial component and temporal component of the wave, corresponding to pump wave ω_p or Stokes wave ω_S.

Note that

$$G_{p,S}(\mathbf{r}) = \hat{g}(\mathbf{r}) \cdot e^{ik_{p,S}(\mathbf{r}-\mathbf{r_0})} \tag{3}$$

where $k_{p,S} = n_{p,S} \cdot \omega_{p,S} / c$, c is the speed of light in vacuum. $\mathbf{r_0}$ ($x_0 \hat{x}, y_0 \hat{y}, z_0 \hat{z}$) is the position for the source. ($\hat{x}$, $\hat{y}$, $\hat{z}$) are the unit vectors along the axis x, y, z direction respectively, in the Cartesian axis system. We also employ the Gaussian form to the source:

$$\hat{g}(\mathbf{r}) = \hat{g}(x\hat{x}, y_0\hat{y}, z\hat{z}) = e^{-\frac{(x-x_0)^2}{a_1^2}} \cdot e^{-\frac{(y-y_0)^2}{b_1^2}} \cdot \hat{y} \tag{4}$$

where $a_1 = w/2$, $b_1 = h/2$, and w, h are the width and height of the source. Note that w and h are the distance between the points when the Gaussian function attenuates to (1/e) of the maximum.

The temporal component is defined as:

$$T_{p,S}(t) = e^{-\omega_{p,S} \cdot t} \tag{5}$$

We have used Eqs. (2)–(5) in simulating the electric field profiles of the coupled cavities.

3. Basic structure, simulation method and main operating parameters

In order to enhance Raman lasing or to decrease the threshold power of pump for Raman lasing, we apply resonance enhancement of optical field in PC defect cavities in designing the Raman laser system. Further from Eq. (1), we can see that high quality factors of both the pump and Stokes wave cavities are required to obtain low threshold power of pump for Raman lasing. With these in mind, we configure the structures as shown in Fig. 1.

In the system shown in Fig. 1, there are five coupled cavities: the waveguide cavity marked with purple, and the vertical cavities *VC-1* and *VC-2* marked with yellow and green, respectively. These cavities are coupled together by the dot-cavity at the center of the structure through optical tunneling. The resonance wavelength of the dot-cavity is adjusted by tuning R_3 (R_1, R_2, and R_3 represent the radii of rods 1, 2, 3 respectively). In Fig. 1, l_1 and l_2 are the lengths of the waveguide in vertical cavities *VC-1* and *VC-2* respectively. Port *A* and *B* are for pump, Port *C* and *D* are for outputs.

We need to design coupled micro-cavities, which possess high quality factors for the pump laser mode f_p, and the Stokes mode f_S, as well as for the anti-Stokes mode f_{aS}. In the case of silicon, these two modes need to satisfy the condition [5,11]:

$$\Delta f = f_p - f_S = 15.6 THz \tag{6}$$

For numerical experiments, we solve the full 2D nonlinear Maxwell's equations by FDTD method, with perfectly matched layer boundary conditions. The Courant stable condition is satisfied since the mesh sizes in both the x and z directions are set to be $a/16$, with the time step fixed at 8.33×10^{-2} fs. In the following simulations, we consider a PC of square lattice consisting of circular rods with a lattice period of $a = 575$nm and radius $0.2a$ (except for rods 1, 2, 3 in Fig. 1); the refractive index of the circular rods is $n = 3.4$, and the refractive index of the background air is $n_b = 1$. Furthermore, only TE-mode operation is considered. In TE-mode operation, the electric vector of the wave is perpendicular to the propagation route of waves in the waveguide and parallel to the axis of poles in the PCs.

In the case of a defect-free uniform PC under the above operating parameters, a standard plane-wave expansion method yields a large bandgap: the light with wavelengths between $2.381a$ and $3.509a$ cannot pass through the uniform PCs and thus is completely reflected at the PCs boundary [13]. Since the pump and Raman scattering waves should be confined to propagate in the waveguide, the wavelengths of the pump and Raman scattering waves should be chosen to be within the bandgap of the PCs.
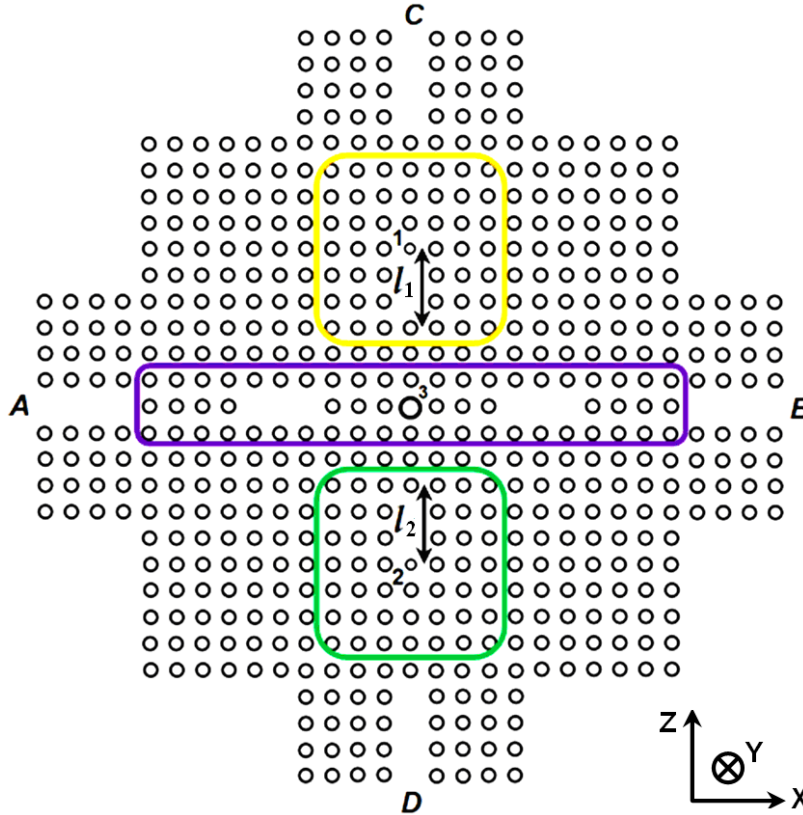
Fig. 1. Schematic of the PC coupled cavities for Raman lasing in silicon. Ports **A** and **B** are for the pump, and **C** and **D** for Raman scattering waves (output); the cavities marked with yellow and green denote **VC-1** and **VC-2**, respectively. The waveguide cavity is marked with purple.

Finally, the difficulty in fabrication should also be taken into consideration in choosing either the air-hole type or the dielectric-rod type [14–20], even though their transmission efficiencies and out-of-plane radiation losses are comparable [20]. Air-hole type PC is easier to fabricate than the latter by using standard pattern generation methods and such a waveguide operates usually in multimode [14]. A bottom up fabrication method is preferred to make rod-type PCs [15] that can be easily operated in single mode. With careful control of the surface roughness and fabrication steps, our design of dielectric-rod type PC with high quality is achievable in practice.

4. The structure emitting Stokes only

We now consider the system shown in Fig. 1 that only emits Stokes. For this purpose, the two vertical cavities should have the same resonant wavelength and be equal to the Stokes wavelength. So, we set $R_1 = R_2$. For being concise, we just consider the structure for emitting Stokes waves. Generally we need to take $l_1 = l_2 = ma$, where $m = 3, 4, 5$, etc, because the lattice period $n_{eff}a$ is set to be about a half of the wavelength of the pump wave and the wavelength difference between the Stokes and pump waves is small. Here n_{eff} is the effective refractive index of the photonic crystal.

As a first example of design (Design **I**), we take $m = 3$. Then we find that, for $R_3 = 0.51a$, by pumping light with the wavelength of 1549.2nm from Port **A** and **B**, we can get Stokes from Port **C** and **D** simultaneously. This is observed by setting a Gaussian impulse at the center of the structure as shown in Fig. 2(a), displaying the pump and Stokes modes by setting a Gaussian impulse at the center of the structure shown in Fig. 1. It is interesting to find that

for the pump, there are two modes rather than one single mode. The explanation is that strong coupling happens in the directly connected sub cavities (dot cavity and waveguide cavities), similar to what was shown in Ref. [21]. Besides, there are two modes in the vertical cavity **VC-1** (and **VC-2**), however according to Eq. (6), only Stokes mode will be excited when the pump wavelength is fixed.
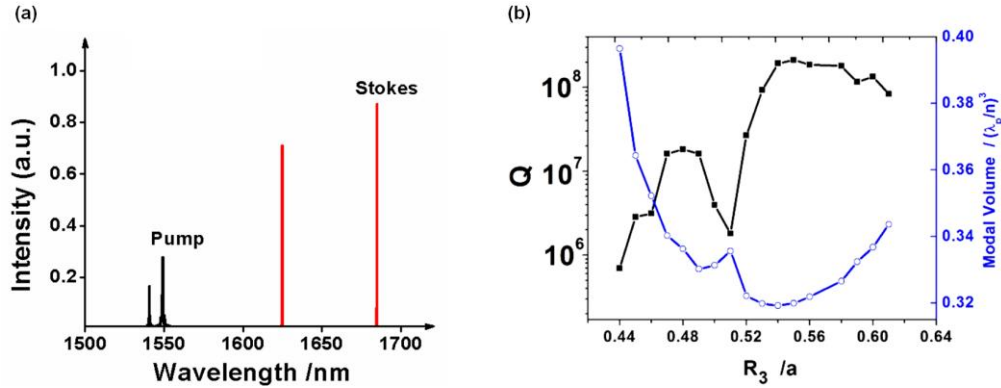

Fig. 2. (a) Resonant frequencies of the pump, and Stokes modes within the photonic band gap for Design (**I**). (b) Q and modal volume for pump as a function of the radius of R_3, while fixing $l_1 = l_2 = 3a$, and $R_1 = R_2 = 0.2a$.

We have used Rsoft's component design suite: *Q-Finder* [12] to obtain Fig. 2(b), which depicts the quality factor Q and modal volume for pump versus R_3. By fixing $l_1 = l_2 = 3a$, and $R_1 = R_2 = 0.2a$, and tuning the radius of R_3 (i.e. tuning the frequency of pump), we obtain such plots. In our further investigation, we tried: $l_1 = l_2 = 2a$, 4a, with $R_1 = R_2 = 0.2a$, which make the size of the vertical cavity **VC-1** (and **VC-2**) to vary; we find that with the increase of l_1 (and l_2), the Q for pump decreases, but still keeps the same order of magnitude for any fixed R_3. In addition, the plot of the modal volume for pump stays the same as shown in Fig. 2(b). This is because the mode of pump f_p is localized in the dot cavity and waveguide cavity; the limited size-change in the vertical cavity **VC-1** (and **VC-2**), which is for capturing the Stokes (or anti-Stokes), can hardly influence the electric field distribution of the pump.

Figure 2(b) shows the quality factor Q versus R_3. We find that there exists a turning point at $R_3 = 0.51a$. This can be explained by the concept of mode matching: the point cavity has the same resonant wavelength as the waveguide cavities at $R_3 = 0.51a$, which makes the coupling to take place among mono-pole type mode in the point cavity and dipole modes in waveguide cavities, as depicted by Fig. 3(a). At $R_3 = 0.54a$, it is important to note that a minimized modal volume of the pump mode $0.3192(\lambda/n)^3$ (as small as $0.03\mu m^3$) could be obtained. Hence ultra-high density of energy is confined in the point cavity, resulting in strong enhancement of the optical fields with wavelength at and near the localized mode. This triggers the Raman scattering process. The reason for the minimized modal volume could be explained as follows: at the point $R_3 = 0.54a$, the coupling between the dot cavity and the waveguide cavity becomes the worst, resulting in less energy-leakage from the dot cavity to the waveguide cavity, thus producing higher Q for the pump.
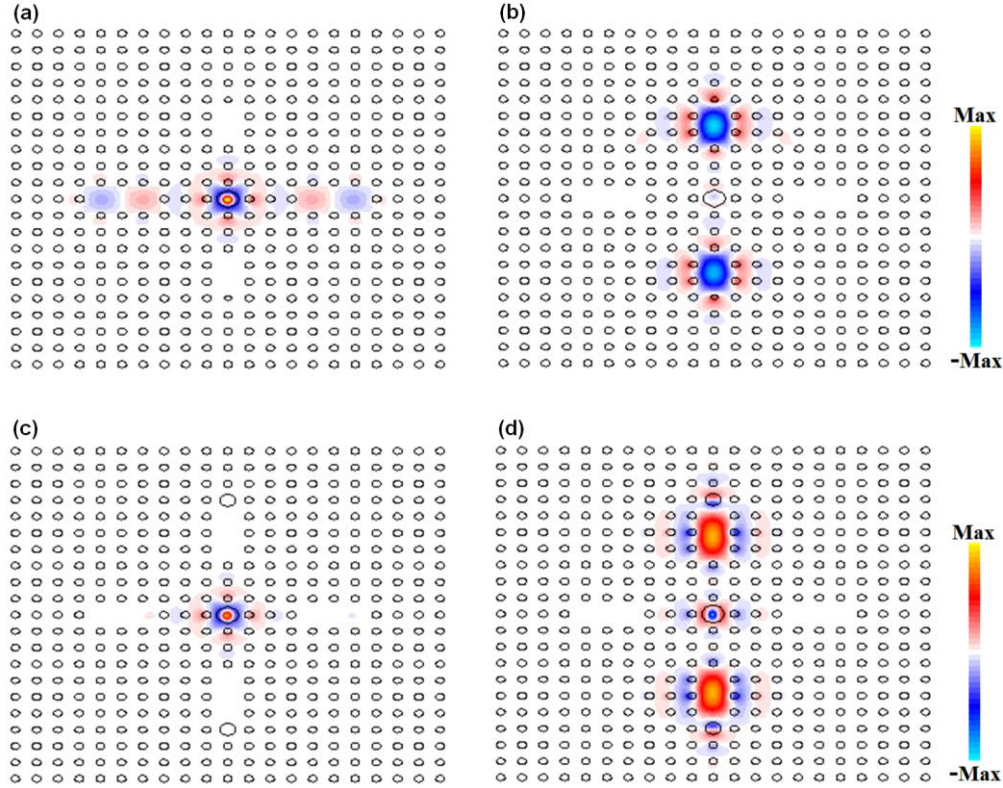
Fig. 3. The electric field profiles of pump mode and Stokes mode: (a) and (b) for Design (**I**); (c) and (d) for Design **II**. The dot cavity and the waveguide cavity share the same resonant wavelength of the pump in (a); (c) describes the worst coupling between the dot and the waveguide cavities. (b) and (d) demonstrate the Stokes modes that are localized in **VC-1** and **VC-2**. The modal overlap ξ of (a) and (b) is much smaller than that of (c) and (d). Note that the simulation shown here was performed with Rsoft's component design suit: *Fullwave* [12], using the definitions given by Eq. (2).

Optimized design parameters used for Design **I** are: $a = 575$nm, $R_1 = R_2 = 0.15a$, $R_3 = 0.51a$, and $l_1 = l_2 = 3a$. The small cavity size and the mutually perpendicular distribution of energy stored in waveguide and vertical cavities result in low modal overlap. The calculated modal overlap integral ξ is only 2.95×10^{-3} between the Stokes and pump modes (see Fig. 3(a) and Fig. 3(b)). As seen from Fig. 3(b), since the Stokes mode is localized in the **VC-1** and **VC-2** cavities, it is not resonant in the dot cavity; this limits the amount of modal overlap ξ. In comparison with the recently reported work (see Ref [5].), the modal overlap in our design is much smaller; however, with the ultra high Q of the pump, Stokes would offset the influence of smaller ξ, which makes the P_{th} decrease by 98.8%. The estimated modal volume for Stokes mode of the coupled cavity is $V_m \sim 2.6214(\lambda/n)^3$ ($\sim 0.319 \mu m^3$) for Design **I**. With the calculated $Q_S = 8.8938 \times 10^5$ at 1684.9nm, the threshold power of pump for lasing of the Stokes in the coupled cavities is estimated to be around 4.24μW, which is based on parameters $g_s = 70$cm/GW [5] and $\xi = 2.95 \times 10^{-3}$. For further improvement, we propose setting an elliptical rod positioned at the center of the dot cavity so that the pump and Stokes could be simultaneously resonant in the dot cavity, which might result in larger modal overlap ξ. Such an approach is meaningful because it may offer an option toward decreasing the P_{th} while still keeping the same range of Q_p and Q_S.

Research on cavity Raman gain enhancement has been conducted by several groups [3,22–26]. For example, Lin [24,25] introduced the effective interaction length L_c expressed

as $L_c = Q_{p,S} \cdot \lambda_{p,S} / 2\pi n_{p,S}$, to estimate Raman gain enhancement. Here, in our simulation, the high-Q (e.g., 8.8938×10^5) of the coupled cavity has an effective interaction length of 70.1mm, a factor of 2.0631×10^4 larger than the physical length (~3.4μm) of the cavity for the Stokes wavelength at 1684.9nm.

As a second example of design (Design **II**), we take $l_1 = l_2 = 4a$. Optimized parameters used in Design **II** are: $a = 553$nm, $R_1 = R_2 = 0.36a$, and $R_3 = 0.54a$. The field distributions are shown in Fig. 3(c) and Fig. 3(d). As seen in Fig. 3(c), the coupling between the dot cavity and the waveguide cavity becomes the worst so that the electric field of pump is localized in the dot cavity, which greatly increases the Q and decreases the modal volume of the pump. Figure 3(d) shows that Stokes mode is mainly localized in **VC-1** and **VC-2**. The threshold power of pump for Stokes lasing could be as small as 53.5nW, which is only 1.26% of that for Design **I**. Here, the dot cavity and the waveguide cavity do not share the same resonant wavelength, resulting in less leakage from the dot cavity thus higher Q for the pump, compared to Design **I**. Moreover, comparing the field profiles in Fig. 3(c) and 3(d) with that in Fig. 3(a) and 3(b), it can be seen that the modal overlap ξ of Fig. 3(c) and 3(d) is much higher than that of Fig. 3(a) and 3(b); this explains why the threshold power for Design **II** is much lower than that for Design **I**, referring to Eq. (1). The operating parameters and properties for Design **I** and **II** are summarized in Table 1.

Table 1. Design summary of PC coupled cavities for Raman lasing (Stokes) in silicon

Design No.	Parameter	Pump	Stokes
	λ (nm)	1549.2	1684.9
	Q	1.7888×10^6	8.8938×10^5
I	$V_m ((\lambda/n)^3)$	0.3413	2.6214
	ξ	N/A	2.95×10^{-3}
	P_{th} (W)	4.24×10^{-6}	N/A
	λ (nm)	1550.4	1686.4
	Q	9.0635×10^7	4.3351×10^4
II	$V_m ((\lambda/n)^3)$	0.3192	2.4877
	ξ	N/A	9.01×10^{-2}
	P_{th} (W)	5.35×10^{-8}	N/A

5. The structure emitting Stokes and anti-Stokes waves simultaneously and separately

We now consider the system shown in Fig. 1 that emits Stokes and anti-Stokes waves simultaneously and separately. We set $l_2 = 2a$ and $l_1 \neq l_2$, so that Stokes goes out from port **C** and anti-Stokes goes out from port **D** in Fig. 1. By fine-tuning the R_2 and R_3, we can get the distinct modes which meet the need of Δf for Raman scattering in silicon.

As a first example of this design (Design **III**), we take $l_1 = 3a$, and the optimized parameters are: $a = 575$nm, $R_1 = 0.15a$, $R_2 = 0.07a$ and $R_3 = 0.51a$. When a Gaussian impulse is launched at the center of the structure, Stokes and anti-Stokes modes are symmetrical with the pump mode as shown in Fig. 4.
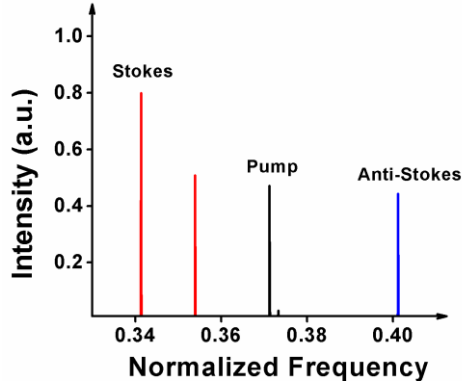
Fig. 4. The normalized resonant frequencies of the pump, Stokes and anti-Stokes modes for Design III. These are within the photonic band gap. The Stokes mode is localized in **VC-1**, while the anti-Stokes mode is in **VC-2**. There exists one extra mode in **VC-1**, however only Stokes mode will be excited when the pump wavelength is fixed, according to Eq. (6).

The estimated modal volumes for Stokes and anti-Stokes mode of the coupled cavity are $V_m \sim 1.3099(\lambda/n)^3$ and $1.1237(\lambda/n)^3$ respectively. Based on parameters $g_s = 70$cm/GW [5], $\xi_{p\text{-}S} = 2.90 \times 10^{-3}$, and $\xi_{p\text{-}aS} = 1.57 \times 10^{-2}$, with the calculated $Q_S = 8.8825 \times 10^5$ at 1684.9nm and $Q_{aS} = 6.9926 \times 10^4$ at 1433.7nm, the threshold power of the pump for Raman lasing in the coupled cavities is estimated to be around 2.15μW (for Stokes) and 3.13μW (for anti-Stokes) respectively, as shown in Table 2.

As a second example of design (Design **IV**), we take $l_1 = 4a$. For Design **IV**, optimized parameters are: $a = 553$nm, $R_1 = 0.36a$, $R_2 = 0.13a$ and $R_3 = 0.54a$. Ultra-low threshold power as small as 17.7nW and 2.58nW can be obtained for the pump to produce Stokes and anti-Stokes lasing respectively. To obtain both lasing simultaneously, the total threshold power should be the sum of the two. Such low threshold is useful for ultra-sensitive devices, especially for applications in biological and medical diagnoses. As reported in Ref. [27], in silicon waveguides, the maximum measured Stokes/anti-Stokes power conversion efficiency is 10^{-5}, resulting in ultra-low output power, which is on the order of nW. In this case, the coupled structure can emit laser at the Raman wavelength and may serve as a sensor to detect such weak signals. In cancer diagnosis, Raman signals (or tissue fluorescence) are usually weak and require sensitive detectors [28], our design could be used to collect optical signals exiting from the sample, with ultra-low threshold lasing which could be easily detected. In particular, our design for the simultaneous and separate signals for Stokes and anti-Stoke emission could be amenable to conducting coherent anti-Stokes Raman scattering (CARS) studies on chemical and biological samples. The pump frequency can be tuned by changing R_3 on multiple cavity designs on the same silicon chip. When the difference between the pump and Stokes frequencies is matched with the molecular vibrational frequency, a strong signal could exit from the anti-Stokes port [29,30].

For getting better insight into the physics of the coupled structure for this case, the electric field profiles of Stokes mode and of anti-Stokes mode are illustrated in Fig. 5. The Stokes mode is localized in the **VC-1**, while the anti-Stokes mode is localized in the **VC-2**, so that the two modes can be easily separated. As demonstrated, the size of **VC-1** is larger than that of **VC-2**, which makes the Stokes wave with a longer wavelength be localized in the top cavity and the anti-Stokes wave with a shorter wavelength in the bottom cavity.

Compared with Design **III**, where $R_3 = 0.51a$, the Q_{aS} increases by a factor of 20. This could be explained as follows: when $R_3 = 0.54a$, normalized anti-Stokes frequency $f_{aS} = 0.3854302$ is further away from the band gap edge ($f_{edge} = 0.419639$) and closer to the bandgap center, resulting in higher quality factor Q and thus lower radiation losses [5].

The operating parameters and properties for Design **III** and **IV** are summarized in Table 2. The threshold power of pump for anti-Stokes lasing is an order of magnitude lower than that for Stokes lasing.
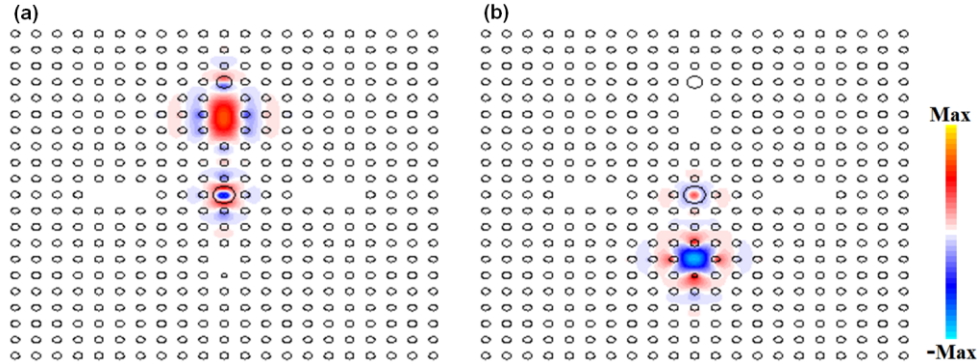

Fig. 5. The electric field profiles of Stokes mode (a) and anti-Stokes mode (b) for Design **IV**.

Table 2. Design summary of photonic crystal coupled cavities for Raman lasing (Stokes and anti-Stokes) in silicon

Design No.	Parameter	Pump	Stokes	Anti-Stokes
III	λ (nm)	1549.2	1684.9	1433.7
	Q	1.7984×10^6	8.8825×10^5	6.9926×10^4
	V_m $((\lambda/n)^3)$	0.3413	1.3099	1.1237
	ξ	N/A	2.90×10^{-3}	1.57×10^{-2}
	P_{th} (W)	2.15×10^{-6}, for Stokes lasing;		
		3.13×10^{-6}, for anti-Stokes lasing.		
IV	λ (nm)	1550.4	1686.4	1434.8
	Q	1.2544×10^8	4.3355×10^4	6.9938×10^5
	V_m $((\lambda/n)^3)$	0.3192	1.2426	0.8561
	ξ	N/A	9.82×10^{-2}	2.08×10^{-2}
	P_{th} (W)	1.77×10^{-8}, for Stokes lasing;		
		2.58×10^{-9}, for anti-Stokes lasing.		

6. Conclusion

In this work we have presented the conceptual design of coupled cavities in two-dimensional rod-type photonic crystals for enhancement of stimulated Raman lasing in silicon. Specifically, we have numerically designed five coupled sub cavities to obtain high *Q* factor and low modal volume resulting in ultra-low threshold lasing, and to support the required pump-Stokes and pump-anti-Stokes modal spacing in silicon PC. This conceptual design may offer an option towards fabricating all-optical monolithic silicon devices. Our design is also useful for biological and medical sensors.

Acknowledgments